Satellite remote sensing of boreal forest and wetland vegetation cover and change

Franklin, S., Ahmed, O., Wasson, R., Stefanuk, M., Skeries, E., and G. Williams

Summary

Classification accuracy of four wetland cover types was 91% overall based on a combination of airborne LiDAR DEM-derived geomorphometrics, Radarsat-2 and Landsat-8 satellite sensor data in northern Ontario. This was a significant improvement over the classification accuracy obtained using either satellite sensor data set alone (84%). Individual fen, bog, swamp and upland forest classes were the most accurate following PCA data fusion of the Radarsat-2 and Landsat imagery, and the use of gravity-, solar- and wind-field geomorphometric derivatives such as 'topographic openness', terrain shape indices, and surface insolation. Results from the Hearst Forest Management Area demonstrated that the Landsat time series change detection protocol was 90% accurate for three stand-replacing forest changes, and 75% for four non-stand replacing changes. Preliminary tests in the Alberta Oil Sands Region confirmed these accuracies. Adjusting the change threshold improved initial seismic line detection accuracy to 65% (±10%).

Research Statement

To determine change detection and classification accuracy of selected wetland and forest land cover and disturbance classes in three different boreal forest study areas using combinations of Radarsat-2, Landsat time series, and airborne LiDAR-based DEM geomorphometrics.

Study Areas

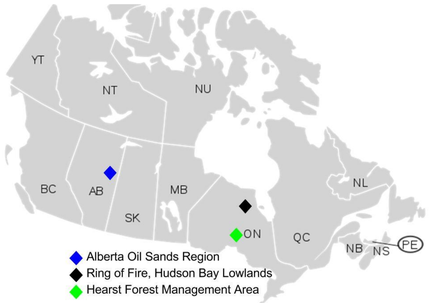

Figure 1. Location of the three study areas.

Alberta Oil Sands Region

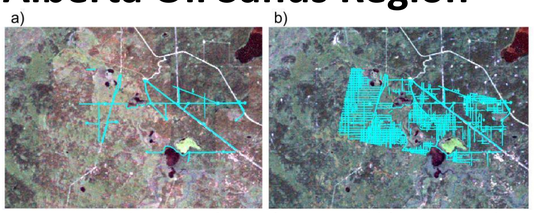

Figure 2. Landsat data from a) 2010 and b) 2011 overlain with change data acquired from ABMI showing new seismic lines features that were undetected in the initial time series protocol.

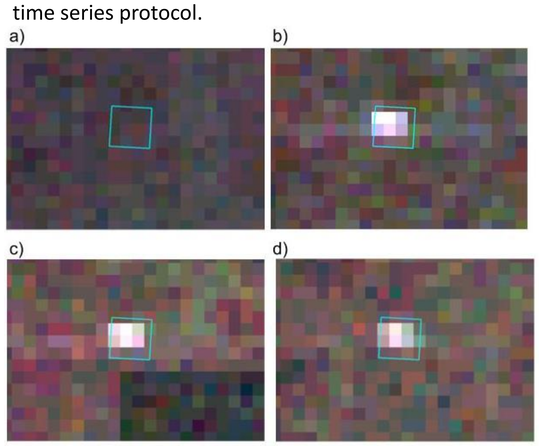

Figure 3. Landsat data from 1984 to 1987 (a-d), with 1985 wellsite feature from ABMI dataset overlain. Though this feature persisted for many consecutive years, even beyond those shown, and was discerned in the imagery, it was undetected in the initial time series protocol.

Hudson Bay Lowlands Ring of Fire Area

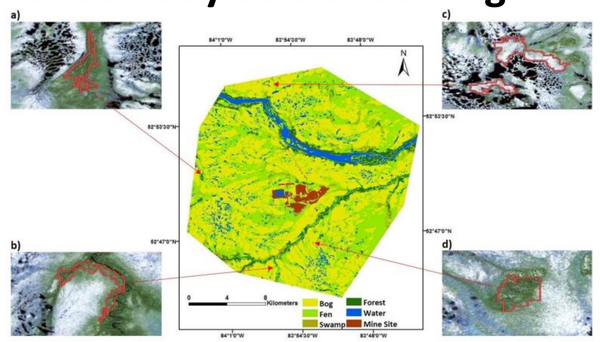

Figure 4. Final wetland classification map showing distribution of wetland classes at 91.78% overall classification accuracy using all available Radarsat-2, Landsat-8 and LiDAR DEM-derived geomorphometric variables. Selected examples of four wetland class training areas and segments overlaid on high spatial resolution WorldView-2 reference imagery a) forest, b) fen, c) bog and d) swamp

		Bog		Fen		Swamp		Forest		Water	
Overall Accuracy (%)	Margin of Error ± (%)	P.A. (%)	U.A. (%)	P.A. (%)	U.A. (%)	P.A. (%)	U.A. (%)	P.A. (%)	U.A. (%)	P.A. (%)	U.A. (%)
Radarsat	80.92	3.19	93.44	87.02	64.86	72.72	48.38	65.21	86.11	68.88	92.68	97.43
Landsat	84.48	3.06	94.26	92.74	78.38	74.36	58.06	66.66	80.56	85.29	90.24	90.24
Radarsat and Landsat	86.51	2.94	95.90	77.92	81.08	77.92	58.06	69.23	83.33	85.71	92.68	92.68
Radarsat, Landsat, Elevation, Slope, Aspect	87.82	2.90	95.90	77.92	85.13	79.74	58.06	69.23	86.11	86.11	92.68	92.68
Geomorp-hometry	78.61	3.17	91.80	84.21	60.81	68.18	38.70	70.58	91.66	76.74	90.24	82.22
All Combined	91.78	2.81	95.90	95.90	90.54	88.15	74.19	82.14	91.66	86.84	91.66	86.84

Table 1. Classification accuracy summary table based on 321 training samples and different combinations of variables in the Random Forest classifier following the out-of-bag (OOB) method. Individual class accuracies displayed significant variation based on the input variables. User's accuracy varied between 77% and 95% with different spectral response inputs.

Hearst Forest Management Area

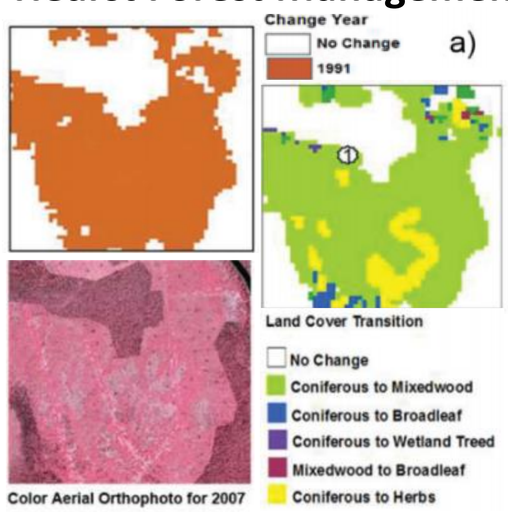

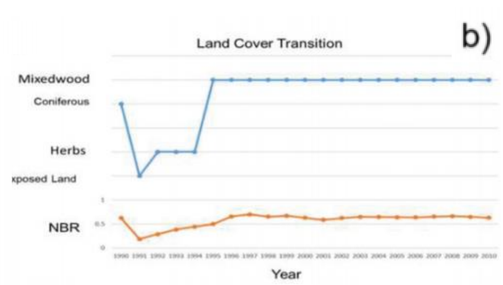

Figure 5. Example of: a) land cover transition at a site that was clearcut at the beginning of the available time series and subsequently converted to predominantly mixedwood at the end of the time series; b) shows the transition for a pixel located near the edge of this cutover where the land cover transitioned from coniferous to exposed land, then to herb, and finally to the mixedwood forest class.

Methods

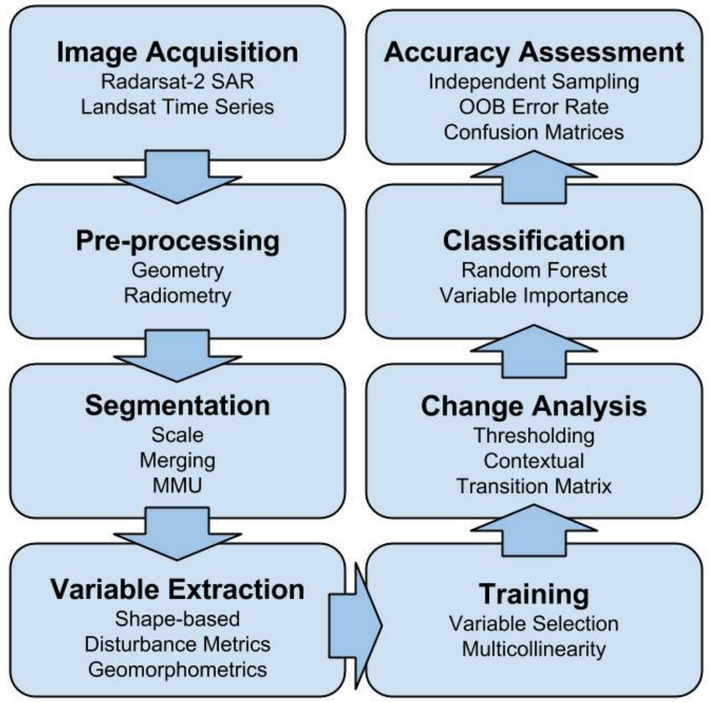

Figure 6. Generalized methods flow chart.

Papers Published/Submitted/Presented

Published: Photogrammetric Engineering and Remote Sensing; International Journal of Remote Sensing.
In Review: Progress in Physical Geography; GIScience and Remote Sensing; Canadian Journal of Remote Sensing.
Presentations: ASPRS Imaging and Geospatial Technology Forum, Fort Worth, Texas (April 2016); 37th Canadian Symposium on Remote Sensing, Winnipeg (June 2016).

Acknowledgements

This research was supported by a Natural Sciences and Engineering Research Council of Canada Collaborative Research and Development Grant (CRDPJ 469943-14) in conjunction with Alberta-Pacific Forest Industries, Cenovus Energy, and ConocoPhillips Canada. The Canadian Space Agency and Canadian Forest Service are thanked for their support.